Intermediate-velocity atomic collisions. V. Electron capture and loss in C^{3+} and O^{5+} collisions with H_2 and He

E. C. Montenegro and G. M. Sigaud
Departamento de Física, Pontifícia Universidade Católica do Rio de Janeiro, Caixa Postal 38071, 22453 Rio de Janeiro, Rio de Janeiro, Brazil

W. E. Meyerhof
Department of Physics, Stanford University, California 94305
(Received 5 August 1991)

Electron-capture and -loss cross sections in C^{3+} and O^{5+} collisions with H_2 and He are measured in the 1.5- to 4.0-MeV energy range. The results for projectile electron loss are compared with the plane-wave Born approximation including the interaction between target and projectile electrons. It is shown that such single-channel analysis is not sufficient to explain the results, but that projectile electron loss, electron capture by the projectile, and target ionization must be considered together to interpret the data. This interpretation allows one to extract the electron-capture probability at small impact parameters. A theoretical estimate based on the independent-particle model and the decay model to unitarize the electron-capture and target-ionization probabilities is described. This analysis explains the main features of the cross sections involved as well as the electron-capture probability at small impact parameters.

PACS number(s): 34.50.Fa

I. INTRODUCTION

This work is a sequel to previous studies [1–4] on electron ionization, excitation, and capture in ion-atom collisions in a velocity regime intermediate between low velocities, where the molecular model is applicable, and high velocities, where atomic or pertubative models are useful [5]. The present work concerns projectile electron loss in the presence of other collision channels which have a strong influence on the electron-loss cross sections.

In the simplest cases, a single-channel analysis is sufficient to explain the experimental results, such as the application of the plane-wave Born approximation (PWBA) to projectile one-electron loss. In these cases, the loss process is due basically to the Coulomb interaction between the target nucleus and the active projectile electron. However, for light targets such as H_2 or He, the role of the target electrons cannot be ignored. As Bates and Griffing first showed [6], target electrons can play a dual role: if they stay in the ground state during the collision, they screen the target nucleus, thereby decreasing the electron-loss cross section (screening process). If they are excited or ionized, they can produce additional electron loss (antiscreening process). These effects have been studied experimentally [1,7–9] and theoretically [10–15] in the past few years.

However, previously it was shown that in the intermediate-velocity regime electron loss and capture may have to be considered simultaneously [4]. From a strictly theoretical point of view, this would require a coupled-channel calculation, but this procedure is far from being straightforward at intermediate velocities. Simpler approaches are useful in this context, such as that described by Siderovich and co-workers [16,17] and employed by Müller *et al.* [18] in their extensive study of multiple electron capture and target ionization. Here, multichannel effects are taken into account through unitarity considerations within the independent-particle model framework. In the present work, we extend these procedures to cases where not only electron loss and charge transfer are coupled, but where also target ionization influences the charge-transfer probability. In other words, to explain the present experimental findings, it is necessary to couple electron loss by the projectile, ionization of the target, and charge transfer from target to projectile.

II. EXPERIMENTAL PROCEDURE AND RESULTS

Figure 1 shows a general sketch of the experimental arrangement. Beams of C^+, O^+, or O^{2+} with energies from 1.5 to 4 MeV are delivered by the 4-MV Van de Graaff accelerator at the Catholic University of Rio de Janeiro, and stripped to higher charge states by a 10–20-$\mu g/cm^2$ carbon foil. The C^{3+} or O^{5+} beams emerging from the stripper are selected by the switching magnet before entering the experimental line and are collimated through the gas cell. In the gas cell, some fraction of the incoming beam undergoes charge-changing collisions. Three different charge states are analyzed (second analyzing magnet) and recorded by three detectors housed in a detection chamber.

With no gas in the cell, the background pressure in the line behind the switching magnet is less than 2×10^{-6} torr. The gas cell has a volume of approximately 800 cm^3

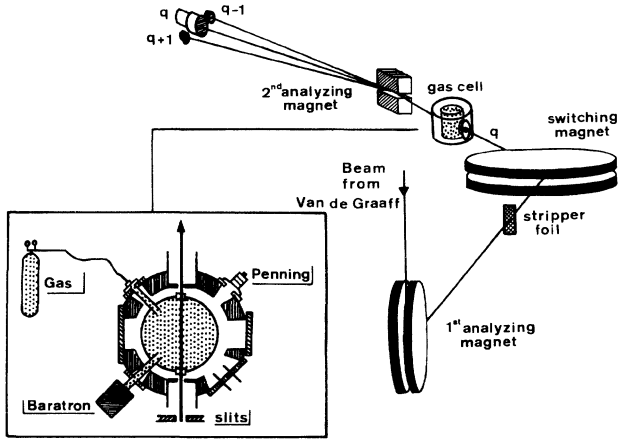

FIG. 1. Sketch of the experimental arrangement, with the target chamber in the inset. The selected beam of charge q and the charge-changed beams of charge $q-1$ and $q+1$ are indicated.

and is placed inside a larger chamber with a 4-in. diffusion pump. This pump and two other diffusion pumps at the entrance and at the exit of the chamber keep the pressures outside and inside the gas cell below a ratio of 1:300. The pressure in the gas cell is measured by an absolute capacitance manometer (MKS-Baratron). The pressure outside the gas cell is monitored by a Penning gauge.

The gas is bled into the cell through a needle valve and can leave it by two 1.8-mm-diam apertures. These apertures together with two other 2.2-mm-diam apertures at the entrance and exit of the scattering chamber allow an efficient differential pumping. The distance between the two cell apertures is 6.5 cm, which gives 6.8 cm for the effective length of the cell [19].

Before entering the scattering chamber, the beam is collimated by two pairs of crossed slits to produce a square cross section of 0.6 mm on the side. In the detection chamber, 3 m downstream from the scattering chamber, the beam has a 1-mm^2 spot. For a beam of charge q, the detection of the $q+1$ and $q-1$ charge states is by means of two surface barrier detectors with a 50-mm^2 active area. The intense entering charge state q is recorded by a photomultiplier tube in front of which is placed a ZnS foil. To increase the light collection efficiency, an Al foil is placed in front of the ZnS. The three detectors are spaced 2.5 and 2.0 cm apart for C^{3+} and O^{5+} impinging beams, respectively.

The efficiency of the surface barrier detectors is assumed to be 100%. The efficiency of the photomultiplier arrangement is determined by moving the position of the detection chamber so that two sets of measurements $\{q-1,q,q+1\}$ and $\{q-2,q-1,q\}$ can be obtained in the three detectors. By taking the ratio of the charge fractions y_q/y_{q-1} for the two cases, the efficiency of the photomultiplier arrangement can be obtained. This efficiency ranges from 0.75 to 0.95 with an average uncertainty of 7%, as the projectile energy varies from 1.5 to 4.0 MeV.

The purity of the target gases as claimed by the manufacturer [20] are 99.999% for H_2 and 99.995% for He. To improve the purity of the He gas in the target cell, the He is passed through a liquid nitrogen trap located in front of the gas feed to the cell. The gas cell and the scattering chamber are kept under high vacuum for at least three days before the data taking, to reduce the effect of outgassing. An estimate of the contribution from the impurities to the measured cross sections is not straightforward because there is no simple scaling law for capture and loss at these energies. If we assume a Z^2 law for loss (which overestimates the contribution for high-Z atoms because of the binding effect [1,4]) and a Z scaling for capture (from electron statistics) as the data from Ref. [1] suggest, we find that the uncertainty in the cross section due to the gas purity lies between 3% and 5% for loss and below 1% for capture.

In our experiments, the cross sections are obtained by the growth rate method. Because K-shell loss cross sections are much smaller than the cross section for the $2s$ electron loss, and because the double-capture cross section is much smaller ($<10\%$ at the lowest energy measured) than the single capture, the beam emerging from the gas cell can be assumed to consist of three charge states only. The charge fractions $y_{q'}$ are obtained from the number of counts $n_{q'}$ in each of the three detectors by

$$y_{q'}=n_{q'}/(n_{q-1}+n_q+n_{q+1}) , \quad (1)$$

where q' is $q-1$ or $q+1$ and n_q are the efficiency corrected counts in the photomultiplier detector.

TABLE I. Charge-changing cross sections for C^{3+} and O^{5+} ions in H_2 and He. All cross sections are given in Mb.

	C^{3+}				O^{5+}			
	H_2		He		H_2		He	
E (MeV)	σ_{34}	σ_{32}	σ_{34}	σ_{32}	σ_{56}	σ_{54}	σ_{56}	σ_{54}
1.5	11.1±1.1	166±18	11.4±1.2	184±22				
2.0	12.9±1.3	66±7.0	14.5±1.6	101±12	1.6±0.2	597±66	1.2±0.1	448±54
2.5	14.9±1.5	32.5±3.5	15.9±1.7	58.6±7.0	2.4±0.2	283±31	2.4±0.3	289±35
3.0	13.6±1.4	17.3±1.9	17.8±2.0	38.1±4.6	3.7±0.4	241±29	3.3±0.4	229±27
3.5	13.5±1.3	9.1±1.0	17.7±1.9	24.8±3.0	4.1±0.4	107±1.2	4.2±0.5	183±22
3.75			16.3±1.8	18.8±2.3				
4.0	12.2±1.2	5.3±0.6	17.5±1.9	15.8±1.9	5.2±0.5	50.4±5.5	5.3±0.6	91.2±11

The cross section $\sigma_{qq'}$ is obtained from the slope of a least-squares straight-line fit of the measured charge fractions as a function of the gas pressure. For capture, where some of the measured charge fractions are higher than 6%, a second-order polynomial gives a better general fit to the data, but this procedure does not change significantly the resulting value of the cross section as compared with a linear fit. At each energy, besides the background, measurements are made at least at four different pressures, and in all cases, the range of measured pressures is kept low enough to assure that no significant double collisions are present.

Table I presents our results. The main sources of uncertainties come from the gas purity (1–5%), photomultiplier efficiency (~7%), background fluctuations (~2%), and effective length of the cell (~5%). The total uncertainties in Table I range from 9% to 12%.

III. PROJECTILE ELECTRON LOSS

Figures 2 and 3 compare our measurements of the one-electron-loss cross section σ_{loss} with other experimental results and theoretical calculations including only the screening and antiscreening processes. The high-energy data for C^{3+} and O^{5+} projectiles are from Refs. [1] and [21], respectively. Figure 2 also shows the $C^{3+}+H_2$ low-energy data of Goffe, Shah, and Gilbody [22], which is in excellent agreement with our results. The theoretical calculations in Figs. 2 and 3 for K- and L-shell projectile one-electron loss use the PWBA theory of Montenegro and Meyerhof [13].

As mentioned in the Introduction, in the PWBA calculation for projectile electron loss by a structured target, such as a hydrogen atom, one distinguishes processes in which the target electron remains in its ground state and in which this electron is excited or ionized [6]. The latter part, which is called the antiscreening effect, requires a summation over all excited states of the target electron. This sum can be worked out only for the hydrogen atom [6]. For targets with two or more electrons, one typically makes diverse assumptions about a mean target excitation energy and can thus execute the sum by using the closure approximation [10,12]. As noted by Anholt [11], this approximation neglects important kinematic effects near the threshold velocity where a free electron would ionize the target. The theory of Montenegro and Meyerhof considers these effects by carrying the approximation for the summation over the target final states up to higher order in its dependence on the excitation energy. In this theory, we used the ionization energies given by Huang [23] with effective projectile charges obtained from Slater rules [24]. This procedure gives $Z_{1L_1}=4.3$, $Z_{1K}=5.7$, $\theta_{L_1}=1.04$, and $\theta_K=0.82$ for C^{3+} and $Z_{1L_1}=6.3$, $Z_{1K}=7.7$, $\theta_{L_1}=1.02$, and $\theta_K=0.86$ for O^{5+}, where $\theta_s=I_s/n_s^2R_\infty$ (I_s=ionization energy of the s subshell, n_s=principal quantum number of the corresponding shell). The theoretical model also needs the target elastic form factor. For He, this was obtained from Salvat *et al.* [25], while for H_2, we used the Stewart molecular form factor as described by Meyerhof *et al.* [14]. The solid curves in Figs. 2 and 3 represent the calculated screening plus antiscreening contributions to the one-electron-loss cross sections, while the dashed curves are

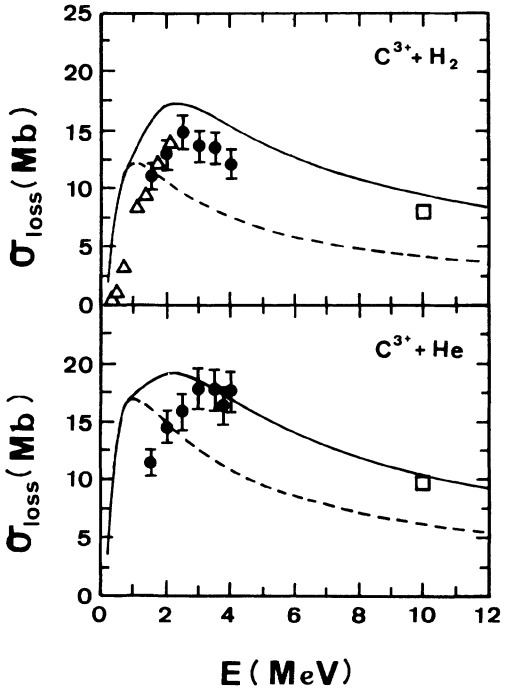

FIG. 2. Projectile one-electron-loss cross sections for C^{3+} on H_2 and He. Experiment: solid circles, this work; open squares, Ref. [1]; open triangles, Ref. [22]. Theory: dashed curve, screening; solid curve, screening plus antiscreening (Ref. [13]).

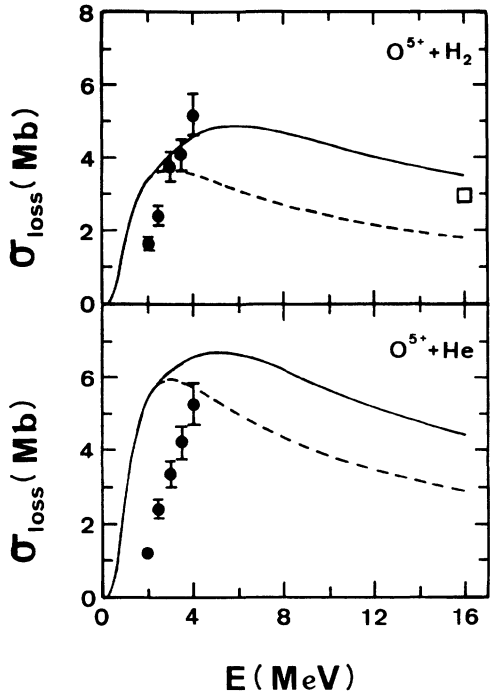

FIG. 3. Projectile one-electron-loss cross sections for O^{5+} on H_2 and He. Experiment: solid circles, this work; open square, Ref. [21]. Theory: same as Fig. 2.

the screening contributions alone. In our measured energy range, the K shell contributes less than 15% to the total electron-loss cross sections. This is included in the calculations.

Comparison of experiment and theory shows that for energies above the cross-section maximum the experimental data appears to be well described by the PWBA screening-antiscreening theory. This behavior was also observed by Hülskötter *et al.* [8] for $1s$ electron loss. Here, it is corroborated for $2s$ electron loss, for the first time. But, it is also clear that for energies below the cross-section maximum, the experimental data decrease faster than the theory. This behavior can be attributed to a possible failure of the PWBA in the low-energy region or to the presence of other collision channels which modify the experimental outcome. In the following section we explore the second possibility, assuming that a modified theoretical model for the screening-antiscreening process can be used in the intermediate- to low-velocity regime. In the Appendix, we examine the question of the validity of the PWBA in the present situation.

IV. MODIFIED ELECTRON-LOSS MODEL

In the following, we try to consider more carefully the states of ionization of the two-electron target (H_2 and He) and the possible electronic processes which could occur. It is important to realize that the measured cross sections do not discriminate between the final target charge states, only between the projectile charge states. In other words, the cross sections for projectile loss (σ_{34} or σ_{56}) correspond to the processes

$$A^{q+}+B^0 \rightarrow A^{q+1}+\begin{cases} B^0+e\ , & \text{single loss} \\ B^{1+}+e+e\ , & \text{loss plus single ionization} \\ B^{2+}+2e+e\ , & \text{loss plus double ionization}\ , \end{cases}$$

while the cross sections for electron capture (σ_{32} or σ_{54}) correspond to

$$A^{q+}+B^0 \rightarrow A^{q-1}+\begin{cases} B^{1+}\ , & \text{single capture} \\ B^{2+}+e\ , & \text{capture plus ionization}\ , \end{cases}$$

where A is C^{3+} or O^{5+} and B stands for He or H_2, and "loss" refers to the projectile, whereas "ionization" refers to the target.

For the particular combinations of collision partners and energies studied in this work, electron capture is a much more probable process than electron loss. As a consequence, electron loss is often accompanied by electron capture in the same collision event, resulting in a final charge state equal to the initial one. Naturally, such a process is not identified as an electron loss in our measurements since the signature of electron loss is the detection of a $q+1$ charge state. Hence, our experimental results must be compared with theoretical predictions where the exclusion of the electron capture associated with projectile electron loss is explicitly considered.

In the screening mode, the electron loss occurs by the action of the screened Coulomb field of the target nucleus [see Fig. 4(a)] and there are two target electrons (of He or H_2) available for capture. If one of them is captured, the event is not registered in the $(q+1)$ detector but in the q detector.

The antiscreening contribution is due to the electron-electron interaction involving one active projectile electron which will be lost and one target electron which will be transferred to another bound or unbound state of the target [see Fig. 4(b)]. Hence, only one target electron is available for capture in a single-step process.

Finally, there is the possibility that a double Auger transition follows capture, a situation that gives the same charge state as the single loss. However, this process has a negligible probability [26] as compared to single-electron loss and can be neglected.

From the above discussion, the cross section for electron loss must be written as

$$\sigma_{\text{loss}}=2\pi\int_0^\infty db\, b(1-P_c)^2 P_{\text{screen}} + 2\pi\int_0^\infty db\, b(1-P_c)P_{\text{anti}}\ , \tag{2}$$

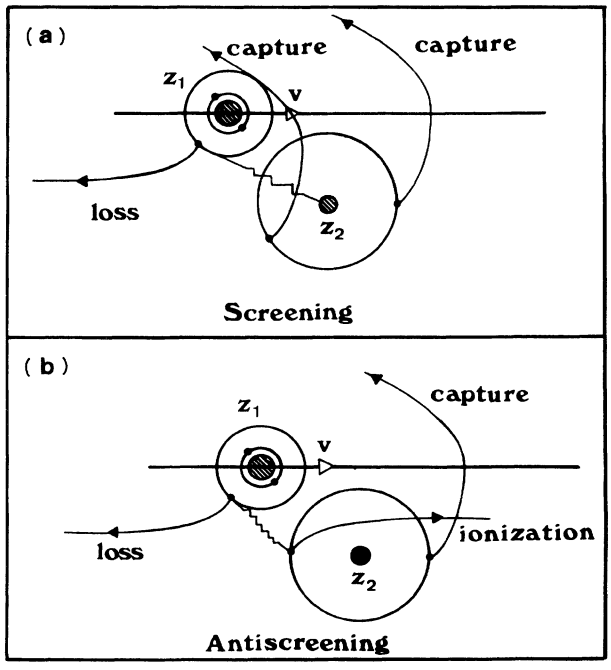

FIG. 4. Illustration of possible electronic processes occurring simultaneously with projectile electron loss when the latter is due to the (a) screening or (b) antiscreening processes.

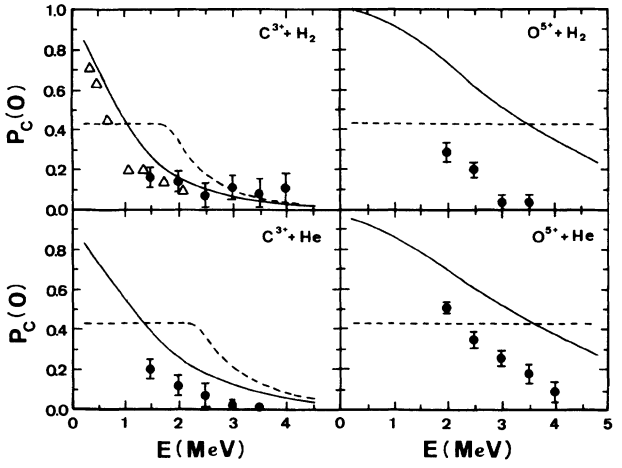

FIG. 5. One-electron-capture probability at zero impact parameter for C^{3+} and O^{5+} ions on H_2 and He. The semiempirical points are obtained using Eq. (3): solid circles, this work; open triangles, Ref. [22]. Theory: the solid curve uses the unitarization procedure of Ref. [17]; the dashed curve is calculated assuming that p_c or p_i is 0.999 wherever the computed values exceed unity.

where P_{screen} and P_{anti} are the screening and antiscreening probabilities for electron loss, respectively, and P_c is the probability for capture of one target electron. Since the loss probabilities range up to values of impact parameters characteristic of the projectile dimensions ($Z_1=6,8$) whereas capture probabilities extend to impact parameters characteristic of the target ($Z_2=1,2$), P_c can be approximated by its value at $b=0$. This yields

$$\sigma_{\text{loss}}=[1-P_c(0)]^2\sigma_{\text{screen}}+[1-P_c(0)]\sigma_{\text{anti}}\ , \tag{3}$$

where σ_{screen} and σ_{anti} are the calculated screening and antiscreening contributions to the one-electron-loss cross section.

Equation (3) gives a simple qualitative explanation for the behavior of the experimental data shown in Figs. 2 and 3. At high energies, the capture probability is small, $P_c(0)\ll 1$ and $\sigma_{\text{loss}}=\sigma_{\text{screen}}+\sigma_{\text{anti}}$. In the intermediate- to low-velocity regime, $P_c(0)$ cannot be neglected and $\sigma_{\text{loss}}<\sigma_{\text{screen}}+\sigma_{\text{anti}}$. If we assume that in this transition energy region σ_{screen} and σ_{anti} can still be calculated in the same way as at higher energies, Eq. (3) can be used to obtain $P_c(0)$ in a semiempirical manner. Using the same values for σ_{screen} and σ_{anti} as in Figs. 2 and 3, the values for $P_c(0)$ so extracted from the experimental data are shown in Fig. 5. A smoothly decreasing trend with increasing energy is found. The meaning of the curves shown is discussed in the next section.

V. ELECTRON CAPTURE AND TARGET IONIZATION

The preceding part of this paper constitutes the main purpose of this study. Nevertheless, since for the collisions we have studied data are now available for projectile electron loss, for target ionization [27], and for electron capture (cross sections [22,27] and probabilities at zero impact parameter), we are tempted to try a consistent three-channel analysis of all this data. Such an attempt has not been made before, as far as we are aware. Hence, although we are only partly successful, we present the results of our analysis.

We begin by examining the capture probability and then the target ionization probability, before evaluating the corresponding cross sections.

Capture from the target and target ionization have high probabilities at intermediate velocities, as was mentioned in Sec. IV, and the theory must maintain unitarity. Hence, projectile loss, capture, and target ionization must be analyzed together. So far, no theory is available for this purpose. To interpret our results, we describe a simple, approximate procedure to obtain quantitative estimates for the relevant cross sections through a combination of unitarization methods and the independent-particle model.

In the following, we consider four kinds of probabilities which we introduce here for purpose of clarification. (i) The single-channel probabilities $p_i(b)$ and $p_c(b)$ for target-electron ionization and capture, respectively, are each calculated ignoring any other collision channel. (ii) The unitarized single-electron probabilities $P_i(b)$ and $P_c(b)$ are calculated considering that the ionization and capture channels are coupled for each target electron. (iii) The probability $P_{m,n}(b)$ for m-fold capture and n-fold ionization for an N-electron target is calculated with the independent-particle model. (iv) The experimentally observed single-electron target ionization and capture probabilities for a two-electron target are denoted by $P_{si}(b)$ and $P_{sc}(b)$, respectively.

The failure of first-order perturbation theory for ionization and capture of light atoms by highly charged projectiles becomes apparent if the corresponding probabilities exceed unity. At intermediate velocities, this can happen to the capture and to the target ionization probabilities at small impact parameters b. Under these conditions, a coupled-channel analysis would be an appropriate theoretical approach. However, instead of coupling amplitudes, a simpler, approximate, procedure can be attempted by coupling the probabilities to obtain unitarization.

Such a procedure was proposed by Sidorovich, Nicolaev, and McGuire [16] through the decay model which assumes that the electron in the initial state of the target can decay alternatively via the ionization or capture channels. As noted above, if $p_i(b)$ and $p_c(b)$ are the single-particle probabilities for target ionization and capture, respectively, the corresponding unitarized probabilities as given by this model are [16–18]

$$P_i(b)=\frac{p_i}{p_i+p_c}(1-e^{-(p_i+p_c)})\ , \tag{4}$$

$$P_c(b)=\frac{p_c}{p_i+p_c}(1-e^{-(p_i+p_c)})\ . \tag{5}$$

In the above formulas, the single-particle ionization probabilities were calculated using the semiclassical approximation [28] with the projectile charges $Z_1=6$ and 8

for C^{3+} and O^{5+} projectiles, respectively. For the He target, the screened nuclear charge was taken as $Z_2=1.7$ and the parameter $\theta=0.586$. The H_2 molecule was considered as a two-electron atom with $Z_2=1.19$ as suggested by Weinbaum's analysis [29] and with $\theta=0.8$ (ionization potential=15.4 eV).

For the single-particle electron-capture probabilities, we used the Oppenheimer-Brinkman-Kramers (OBK) approximation, because of its inherent simplicity and its use in a similar analysis [18]. Nevertheless, we recognize the limitations of the theory in overestimating most cross sections. In order to scale the OBK electron transfer probabilities from $1s\rightarrow 1s$ transitions to other cases, we used a simple scaling law [30,31] rather than more exact expressions [32]. If $p_c(1s-1s,Z_1^*,Z_2^*)$ is the one-electron capture probability from a target $1s$ state with effective charge Z_2^* into a projectile $1s$ state with effective charge Z_1^*, the probability of the electron being captured in a state of the projectile with principal quantum number n, is approximated as follows:

$$p_c(1s-n,Z_1^*,Z_2^*)=2n^2p_c(1s-1s,Z_1^*/n,Z_2^*)\ , \tag{6}$$

where $p_c(1s-1s,Z_1^*/n,Z_2^*)$ is obtained from the OBK approximation [33]:

$$p_c(1s-1s,Z_1^*/n,Z_2^*) =F\frac{2(b/a_0)^4(Z_1^*/n)^5(Z_2^*)^5}{(v/v_0)^2\gamma^2}K_2^2(\gamma^{1/2}b/a_0)\ . \tag{7}$$

In Eq. (7), a_0 and v_0 are the Bohr radius and velocity, respectively, v is the projectile velocity, $K_2(x)$ is the modified Bessel function, and F is an empirical factor to correct the tendency of the OBK approximation to overestimate the cross sections. The parameter γ is given by

$$\gamma=\frac{1}{(v/v_0)^2}\left[\left[\frac{v}{v_0}\right]^4+2\left[\frac{v}{v_0}\right]^2\left[\frac{(Z_1^*)^2}{n^2}+(Z_2^*)^2\right] +\left[\frac{(Z_1^*)^2}{n^2}-(Z_2^*)^2\right]^2\right]\ . \tag{8}$$

Because the final electron state is not determined experimentally, the single-electron-capture probability was obtained by summing Eq. (6) over principal quantum numbers up to $n=20$:

$$p_c=\sum_{n=1}^{20}p_c(1s-n,Z_1^*,Z_2^*)\ . \tag{9}$$

These single-electron capture probabilities were used in Eqs. (4) and (5).

The calculation of Eq. (9) was performed taking $(Z_2^*)^2=(Z_2)^2\theta$ and $Z_1^*=q$, where q is the projectile charge. This choice is justified by the fact that for n values which give the largest contributions to capture, the projectile nucleus can be considered to be completely screened by the projectile electrons.

With the procedure described above, the unitarized capture and target ionization probabilities are obtained through Eqs. (4) and (5). In an N-electron system each electron must choose between being captured with probability P_c, being ionized with probability P_i, or remaining in the target system with probability $1-P_c-P_i$. The probability $P_{m,n}$ for m-fold capture and n-fold ionization of N-independent electrons is obtained by the binomial distribution [16,18]:

$$P_{m,n}=\frac{N!}{m!n!(N-m-n)!}P_c^mP_i^n(1-P_c-P_i)^{N-m-n}\ . \tag{10}$$

Using Eq. (10), with $N=2$, the probabilities of single-electron capture $P_{sc}=P_{1,0}+P_{1,1}$ and of single-electron ionization $P_{si}=P_{0,1}$, can be determined and used to calculate the cross sections for a two-electron target:

$$\sigma_{sc}=2\pi\int_0^\infty db\ bP_{sc}=2\pi\int_0^\infty db\ b2P_c(1-P_c) \tag{11}$$

and

$$\sigma_{si}=2\pi\int_0^\infty db\ bP_{si}=2\pi\int_0^\infty db\ b2P_i(1-P_c-P_i)\ . \tag{12}$$

The corresponding loss cross section is given by Eq. (3).

The value of F which appears in Eq. (7) was adjusted so that the calculated electron-capture cross section at 2.5 MeV agrees with the experimental results of Table I. We obtain $F=0.13$ (C^3+He), 0.38 ($C^{3+}+H_2$), 0.17 ($O^{5+}+He$), and 0.81 ($O^{5+}+H_2$).

As mentioned earlier, at intermediate energies the single-particle probabilities p_i and p_c can exceed unity at small impact parameters, indicating the failure of first-order theories. One simplification introduced by Seaton [34] and used by other authors [35,36] to circumvent this difficulty is to limit the first-order probabilities to some value less than unity. This prescription gives an alternative procedure to calculate the unitarized probabilities. Following Anholt *et al.* [36] we replace p_c or p_i by 0.999 in Eqs. (4) and (5) whenever the corresponding calculated values exceed unity. This gives for the parameter F the values 0.11 ($C^{3+}+He$), 0.20 ($C^{3+}+H_2$), 0.17 ($O^{5+}+He$),

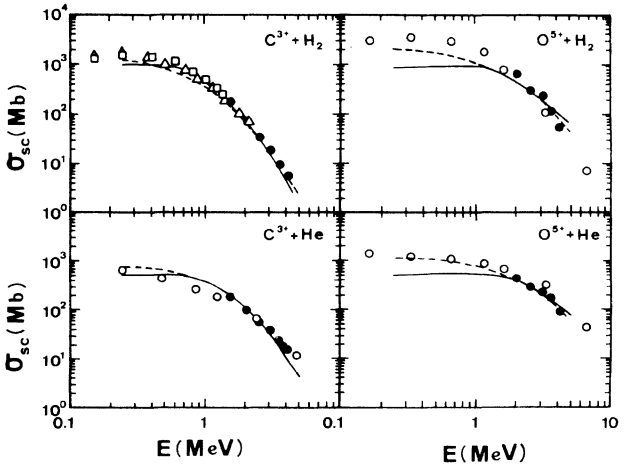

FIG. 6. One-electron-capture cross sections for C^{3+} and O^{5+} ions on H_2 and He. Experiment: solid circles, this work; open triangles, Ref. [22]; open squares, Ref. [37]. The open circles are from the semiempirical fit listed in Ref. [27]. Theory: same as for Fig. 5.

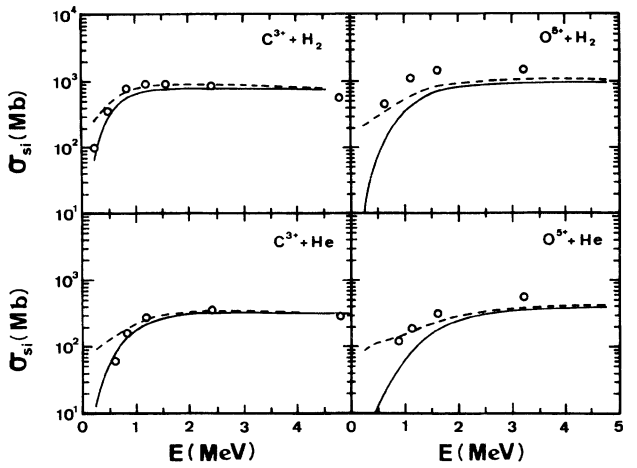

FIG. 7. One-electron target ionization cross sections for C^{3+} and O^{5+} ions on H_2 and He. The open circles are from the semiempirical fit listed in Ref. [27]. Theory: same as for Fig. 5.

and 0.54 ($O^{5+}+H_2$), with the above adjustment procedure.

Figure 6 presents our experimental results and those of others [22,27,37] for single-electron capture together with the present calculations. The solid curves are obtained without any cut on p_c or p_i while the dashed curves limit p_c or p_i to 0.999. Although the trend of the cross-section data is equally well represented by both procedures, if these procedures are applied to $P_c(0)$ (Fig. 5), one sees that the cutoff method of Ref. [36] is not supported by the data. In particular, the $C^{3+}+H_2$, He semiempirical values show good agreement with the present calculations for $P_c(0)$ as given by Eq. (5). At 2.0-MeV projectile energy, our calculations give $p_c(0)=1.37$ and $p_i(0)=7.14$ for $C^{3+}+H_2$, and $p_c(0)=1.86$ and $p_i(0)=5.29$ for $C^{3+}+He$. These probabilities do not violate unitarity too drastically, indicating that reasonable quantitative results can be obtained under these conditions. On the other hand, our $O^{5+}+H_2$,He calculations show only qualitative agreement with semiempirical data for $P_c(0)$. This may be caused by the fact that unitarity is too drastically violated in this case to apply Eq. (5) using first-order theories for $p_c(0)$ and $p_i(0)$. In fact, at 2.0 MeV we find $p_c(0)=35.7$ and $p_i(0)=13.2$ for $O^{5+}+H_2$ and $p_c(0)=28.3$ and $p_i(0)=12.1$ for $O^{5+}+He$.

Figure 7 shows the results of the calculations for target single ionization in comparison with the experimental values given by Janev [27]. The meaning of the curves is the same as in Fig. 6. Although we are not focusing our attention on target ionization, our results illustrate the consistency of the unitarization procedure of Eqs. (4) and (5) together with the independent-particle hypothesis. There is overall qualitative agreement between the calculated results and experiment for both capture and ionization.

VI. COMMENTS AND CONCLUSIONS

The collision regime studied in this work corresponds to a situation where various competing processes occur simultaneously and the analysis of the experimental outcome must take into account all the participating processes. Projectile electron loss, which is the main purpose of our study, depends on capture, which, in turn, depends on target ionization. At present, there is no theoretical treatment which takes into account all these processes in a consistent way. Our strategy was to obtain a quantitative estimate on the basis of first-order theories to indicate the general behavior of the cross sections. Through the combination of these first-order theories with the model of Siderovich and co-workers [16] to enforce unitarity, and with the independent-particle model, we obtain a manageable procedure which gives a general agreement with all the available data.

Our loss measurements with C^{3+} projectiles extend previous data for a H_2 target and provide data for a He target. These measurements, in connection with our interpretation, clearly show the presence of the screening-antiscreening effects also in the electron loss of Li-like ions. Our O^{5+} data lie in an energy region well below the ionization maximum, where electron capture has a major influence in the projectile electron loss.

From the present measurements and calculations of the projectile electron-loss cross section, it is possible to extract semiempirical values for the capture probability at zero impact parameter. To fit these values, we show conclusively that a prescription which simply cuts the first-order probabilities whenever they exceed unity is not valid. This conclusion does not emerge so clearly if only total cross sections are considered. It is apparent from the present analysis that the calculations of the screening and antiscreening contributions to the one-electron-loss cross section in the PWBA framework can be extended into the intermediate-to low-energy region.

ACKNOWLEDGMENTS

The authors gratefully acknowledge comments and suggestions of A. G. de Pinho. This work was supported in part by Conselho Nacional de Desenvolvimento Científico e Tecnológico (CNPq), Fundação de Amparo à Pesquisa do Estado do Rio de Janeiro (FAPERJ), and by National Science Foundation Grant Nos. INT-8900645, PHY-8614650, and PHY-9019293 (Stanford University).

APPENDIX

The PWBA calculation for electron loss can be separated into two independent contributions: screening and antiscreening (see Sec. IV). In this appendix, we discuss briefly the conditions of validity of the PWBA calculations for these two contributions.

For the cases studied in this work, the antiscreening cross section is significant only for energies above 2 MeV in $C^{3+}+H_2$,He and above 4 MeV in $O^{5+}+H_2$,He. Hence, antiscreening practically plays no role in the analysis of our O^{5+} data. For the C^{3+} case, it is apparent from Fig. 2 that for energies above the cross-section maximum where the antiscreening begins to contribute significantly, the PWBA calculations describe our experimental findings well, a result which was observed earlier

by Hülskötter *et al.* [8] for the K-shell loss even near the antiscreening threshold (threshold for free-electron induced electron loss) [11].

Briggs and Taulbjerg [38] have provided criteria for the validity of the PWBA. They suggest that somewhat different criteria apply to the electron-electron interaction (antiscreening) and the nuclear-electron interaction (screening). For the electron-electron interaction, they propose that the PWBA should be valid if

$$v \gg v_{\mathrm{el}} , \tag{A1}$$

where v_{el} is the velocity of the active electron. Equation (A1) implies that the PWBA antiscreening calculations should be used only far from the threshold for free-electron ionization, a condition which, from the above discussion, may be too restrictive. It is also possible that near the free-electron ionization threshold the PWBA antiscreening calculations are not accurate, but here the screening contribution dominates. Consequently, the total cross section is not significantly affected.

For the screened nuclear-electron interaction, Briggs and Taulbjerg suggest a criterion [Eq. (39) of Ref. [38]] which can be written for projectile electron loss in the form

$$v > (Z_1 n_s \theta_s m/M)^{1/3} v_{\mathrm{el}} , \tag{A2}$$

where m/M is the ratio of electronic to the reduced target and projectile masses. This criterion implies that in the present case a PWBA treatment can be applied to the screening part of the loss cross section above a projectile energy of a few tenths of a MeV.

In summary, it is reasonable to suspect that for the systems studied in this paper, the deviation at low energies indicated in Figs. 2 and 3 is not due to the breakdown of the PWBA.

[1] R. Anholt, X. -Y. Xu, Ch. Stoller, J. D. Molitoris, W. E. Meyerhof, B. S. Rude, and R. J. McDonald, Phys. Rev. A **37**, 1105 (1988).

[2] X. -Y. Xu, E. C. Montenegro, R. Anholt, K. Danzmann, W. E. Meyerhof, A. S. Schlachter, B. S. Rude, and R. J. McDonald, Phys. Rev. A **38**, 1848 (1988).

[3] E. C. Montenegro, X. -Y. Xu, W. E. Meyerhof, R. Anholt, K. Danzmann, A. S. Schlachter, B. S. Rude, and R. J. McDonald, Phys. Rev. A **38**, 1854 (1988).

[4] E. C. Montenegro, X. -Y. Xu, W. E. Meyerhof, and R. Anholt, Phys. Rev. A **38**, 3358 (1988).

[5] D. Madison and E. Merzbacker, in *Atomic Inner-Shell Processes,* edited by B. Crasemann (Academic, New York, 1975), pp. 2–69.

[6] D. R. Bates and G. Griffing, Proc. Phys. Soc. London, Sect. A **66**, 90 (1955) and prior references given there.

[7] T. J. M. Zouros, D. H. Lee, and P. Richard, Phys. Rev. Lett. **62**, 2261 (1989).

[8] H. P. Hülskötter, W. E. Meyerhof, E. Dillard, and N. Guardala, Phys. Rev. Lett. **63**, 1938 (1989).

[9] H. P. Hülskötter, B. Feinberg, W. E. Meyerhof, A. Belkacem, J. R. Alonso, L. Blumenfeld, E. Dillard, H. Gould, N. Guardala, G. F. Krebs, M. A. McMahan, M. E. Rhoades-Brown, B. S. Rude, J. Schweppe, D. W. Spooner, K. Street, P. Thieberger, and H. E. Wegner, Phys. Rev. A **44**, 1712 (1991).

[10] J. H. McGuire, N. Stolterfoht, and P. R. Simony, Phys. Rev. A **24**, 97 (1981).

[11] R. Anholt, Phys. Lett. **114A**, 126 (1986).

[12] H. M. Hartley and H. R. J. Walters, J. Phys. B **20**, 1983 (1987).

[13] E. C. Montenegro and W. E. Meyerhof, Phys. Rev. A **43**, 2289 (1991).

[14] W. E. Meyerhof, H. P. Hülskötter, Qiang Dai, J. H. McGuire, and Y. D. Wang, Phys. Rev. A **44**, 5907 (1991).

[15] E. C. Montenegro and W. E. Meyerhof, Phys. Rev. A **44**, 7229 (1991).

[16] V. A. Siderovich, V. S. Nicolaev, and J. H. McGuire, Phys. Rev. A **31**, 2193 (1985).

[17] V. S. Nicolaev and V. A. Siderovich, Nucl. Instrum. Methods Phys. Res. B **36**, 239 (1989).

[18] A. Müller, B. Schuch, W. Groh, and E. Salzborn, Z. Phys. D **7**, 251 (1987).

[19] H. Tawara and A. Russek, Rev. Mod. Phys. **45**, 178 (1973).

[20] S. A. White Martins (Rio de Janeiro).

[21] E. C. Montenegro, W. E. Meyerhof, H. P. Hülskötter, and D. W. Spooner (unpublished).

[22] T. V. Goffe, M. B. Shah, and H. D. Gilbody, J. Phys. B **12**, 3763 (1979).

[23] K. N. Huang, At. Data Nucl. Data Tables **20**, 161 (1977).

[24] J. C. Slater, *Quantum Theory of Atomic Structure* (McGraw-Hill, New York, 1960), Vol. 1.

[25] F. Salvat, J. D. Martinez, R. Mayol, and J. Parellada, Phys. Rev. A **36**, 467 (1987).

[26] M. S. Pindzola and D. C. Griffin, Phys. Rev. A **36**, 2628 (1987).

[27] R. K. Janev, R. A. Phaneuf, and H. T. Hunter, At. Data Nucl. Data Tables **40**, 249 (1988).

[28] J. M. Hansteen, O. M. Johnsen, and L. Kocbach, At. Data Nucl. Data Tables **15**, 315 (1975).

[29] S. Weinbaum, J. Chem. Phys. **1**, 593 (1933).

[30] D. P. Almeida, N. V. de Castro Faria, F. L. Freire, Jr., E. C. Montenegro, and A. G. de Pinho, Phys. Rev. A **36**, 16 (1987).

[31] W. E. Meyerhof, R. Anholt, J. Eichler, H. Gould, Ch. Munger, J. Alonso, P. Thieberger, and H. E. Wegner, Phys. Rev. A **32**, 3291 (1985).

[32] J. Eichler and F. J. Chan, Phys. Rev. A **20**, 104 (1979).

[33] M. R. C. McDowell and J. P. Coleman, *Introduction to the Theory of Ion-Atom Collisions* (North-Holland, Amsterdam, 1970).

[34] M. J. Seaton, Mon. Not. R. Astron. Soc. **127**, 191 (1963).

[35] R. S. Walling and J. C. Weisheit, Phys. Rep. **162**, 1 (1988).

[36] R. Anholt, W. E. Meyerhof, X. -Y. Xu, H. Gould, B. Feinberg, R. J. McDonald, H. E. Wegner, and P. Thieberger, Phys. Rev. A **36**, 1586 (1987).

[37] R. A. Phaneuf, F. W. Meyer, and R. H. McKnight, Phys. Rev. A **17**, 534 (1978).

[38] J. S. Briggs and K. Taulbjerg, in *Structure and Collisions of Ions and Atoms,* edited by I. A. Sellin (Springer, Berlin, 1978), p. 105.